Journal of Alloys and Compounds 515 (2012) 49–56

Contents lists available at SciVerse ScienceDirect

Journal of Alloys and Compounds

journal homepage: www.elsevier.com/locate/jallcom

Synthesis of nanocrystalline yttria powder and fabrication of Cr,Nd:YAG transparent ceramics

Jiang Li*, Wenbin Liu, Benxue Jiang, Jun Zhou, Wenxin Zhang, Liang Wang, Yiqiang Shen, Yubai Pan, Jingkun Guo

Key Laboratory of Transparent Opto-functional Inorganic Materials, Shanghai Institute of Ceramics, Chinese Academy of Sciences, Shanghai 200050, PR China

ARTICLE INFO

Article history:
Received 2 April 2010
Received in revised form 21 October 2011
Accepted 24 October 2011
Available online 1 December 2011

Keywords:
Transparent ceramics
Cr,Nd:YAG
Solid-state reaction
Secondary phase
Nanocrystalline yttria
Precipitation

ABSTRACT

Nanocrystalline yttria powders were synthesized by a precipitation method from yttrium nitrate solution using ammonia water as a precipitant. It was found that the addition of small amount of ammonia sulfate in yttrium nitrate solution can reduce the agglomeration of the produced yttria powders. Y_2O_3 powder with an average particle size of 67 nm was obtained by calcining the precursor at 1100 °C for 2 h. Transparent 0.1 at.%Cr,1.0 at.%Nd:YAG ceramics were fabricated by a solid-state reaction and vacuum sintering with CaO as a charge compensator and tetraethyl orthosilicate (TEOS) as a sintering aid using the prepared Y_2O_3, and the high-purity commercial powders of α-Al_2O_3, Nd_2O_3 and Cr_2O_3 as raw materials. Fully dense Cr,Nd:YAG ceramic with some secondary phase of alumina was obtained by sintering at 1750 °C for 10 h. The average grain size of the sample was about 10 μm and the in-line transmittance was ~52% at 1064 nm, which is lower than the transmission (~82%) of the sample from all-commercial oxide powders. The low transmittance of Cr,Nd:YAG ceramic is mainly caused by the formation of secondary phase due to the non-stoichiometry of the starting powders. In order to overcome the current limitations of the study, weight loss cause by the decomposition of SO_4^{2-} ions and the absorption of water or organic materials in yttria nanopowder should be taken into account.

1. Introduction

Highly transparent Nd:YAG polycrystalline ceramics have gained more and more attention as novel solid-state laser materials due to their several remarkable advantages, such as high doping concentration, easy fabrication of large scale, low cost, multilayer and multifunctional ceramics lasing components, and mass production, compared with Nd:YAG single crystals [1–8]. Laser-diode pumped passively *Q*-switched microchip solid-state lasers with high peak power have been shown to be useful sources for many applications, which has been demonstrated in Cr^{4+},Nd^{3+}:YAG single crystals [9–11]. So by modern ceramic sintering technology, Cr^{4+},Nd^{3+}:YAG transparent ceramics can be fabricated, which may be a more potential self-*Q*-switched laser material used for generating sub-nanosecond laser pulses relative to single crystals with the same composition.

Usually there are two typical methods to fabricate rare earth doped YAG (RE:YAG) transparent. One is solid-state reactive sintering of oxide powder mixture [12–22]. The other way is vacuum sintering of RE:YAG powders synthesize by wet-chemical method [23–29]. In our previous work, transparent Cr^{4+},Nd^{3+}:YAG ceramics were successfully fabricated by solid-state reaction and vacuum sintering [30–32]. The commercial α-Al_2O_3 powders were homogeneous and with average particle size of about 300 nm. The γ-Al_2O_3 powders used were even finer compared with α-Al_2O_3. However, the yttria powders with large agglomerates were of micrometer-size, which may inevitably affect the sinterability and the microstructure of the sample. In the present work, yttria nanopowders with homogeneous particle size were prepared by a wet chemical method, which was similar with the way reported by Wen et al. [33] By using the synthesized yttria powders and the commercial α-Al_2O_3, Cr_2O_3 and Nd_2O_3 powders as raw materials, fabrication of transparent Cr^{4+},Nd^{3+}:YAG ceramics by solid-state reaction and vacuum sintering was investigated. For comparison, Cr^{4+},Nd^{3+}:YAG transparent ceramics have also been fabricated with the same process using large-scaled Y_2O_3 commercial powder and other same starting powders.

2. Experimental

Commercial yttria powder (Shanghai Yulong New Materials Co., Ltd., 99.99%) was dissolved in a high-purity nitric acid (Shanghai Lingfeng Chemical Reagent Co., Ltd., super purity), and then was diluted with deionized water to the concentration of 0.3 M. 2.0 M ammonia water (Shanghai Lingfeng Chemical Reagent Co., Ltd., reagent grade) was used as precipitant and 2.6 g ammonia sulfate was added to a 1250 ml yttrium nitrate solution. The precursor precipitate was synthesized by dripping the

* Corresponding author. Tel.: +86 21 52412816; fax: +86 21 52413903.
E-mail address: lijiang@mail.sic.ac.cn (J. Li).

0925-8388/$ – see front matter © 2011 Elsevier B.V. All rights reserved.
doi:10.1016/j.jallcom.2011.10.083

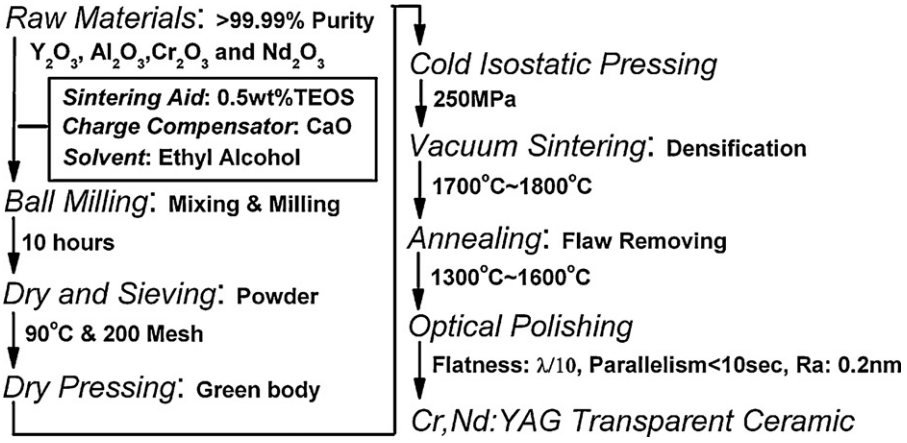

Fig. 1. Solid-state reactive fabrication process of Cr,Nd:YAG transparent ceramics.

ammonia water solution into the mother salt solution at a speed of 3 ml/min under mild agitation. The resultant suspension was aged for 2 h with mild agitation by a magnetic stirrer and the final pH value of the precipitate slurry was 8.0. Then the precipitate slurry was filtered using a suction filter, washed three times with deionized water, rinsed two times with the ethyl alcohol and dried at 90 °C for 24 h. The dried cake was crushed with a corundum pestle and mortar and calcined at different temperatures for 2 h to obtain nanocrystalline yttria powder.

The obtained nanocrystalline yttria powder (or commercial large-sized Y_2O_3 powder) and other commercial high-purity powders of α-Al_2O_3 (Shanghai Wusong Chemical Co., Ltd., 99.99%), Nd_2O_3 (Shanghai Yuelong New Materials Co., Ltd., 99.99%) and Cr_2O_3 (Sinopharm Chemical Reagent Co., Ltd., spectral purity) were used as starting materials to result in a chemical composition of 0.1 at.%Cr,1.0 at.%Nd:YAG. The commercial CaO (Sinopharm Chemical Reagent Co., Ltd., spectral purity) was used as a charge compensator, because Ca^{2+} can balance the charge when Cr^{3+} changes into Cr^{4+}. The commercial tetraethyl orthosilicate (TEOS, Shanghai Lingfeng Chemical Reagent Co., Ltd., spectral purity) was used as a sintering aid. All the composites were mixed by ball-milling with high-purity (99.7%) alumina balls in anhydrous alcohol for 10 h. The mixtures were dried at 90 °C, sieved 200-mesh screen, dry-pressed under 100 MPa into φ20 mm disks and finally cold isostatically pressed under 250 MPa. The compacted disks were sintered at the temperature range of 1600–1780 °C for 10 h in a tungsten mesh-heated vacuum furnace (KZG-110F, Shanghai Chenrong Electrical Furnace Co., Ltd., Shanghai, China) under 3×10^{-3} Pa vacuum during holding. The specimens were placed in a molybdenum crucible. The heating rate was 5 °C/min and the cooling rate was 10 °C/min. The sintered specimens were annealed at 1450 °C for 20 h in air. The solid-state reactive fabrication process of Cr,Nd:YAG transparent ceramics is schematically illustrated in Fig. 1, which is similar with that reported before [34–37]. For cell parameter comparison, 0.1 at.%Cr:YAG and 1.0 at.%Nd:YAG transparent ceramics were fabricated by sintering at 1750 °C for 10 h.

TG–DTA analysis was recorded on a Netzsch STA 449C instrument. Measurements were taken under a continuous flow of air (20 ml min^{-1}). Samples were heated at 10 °C min^{-1} to 1200 °C and then cooled to ambient in air.

Phase identification of powders was performed by a Rigaku D/max2200PC X-ray diffractometer (XRD) using nickel filtered CuK_α radiation (1.5406 Å) in the range of 2θ = 10–80°. The tube current and voltage were 40 mA and 40 kV, respectively. The scanning speed was 4° min^{-1} and the step size was 0.02. The XRD data of powders are refined by Rietveld method using the Maud program (Version 2.30).

The XRD data of ceramics for phase identification were collected at ambient temperature with a HUBER Imaging Plate Guinier Camera G670 [S] (Cu $K_{\alpha1}$ radiation, λ = 1.54056 Å, 40 kV/30 mA, Ge monochromator). The 2θ for all data ranged from 10° to 80° with 0.005° step size. The acquired data are refined by Rietveld method using the Maud program (Version 2.30).

FTIR of the as-prepared precursor and the calcined powders were measured on a Nicolet NEXUS 7000C spectrophotometer in the 400–4000 cm^{-1} range using the KBr pellet (~1 wt% sample) method. Each analysis consisted of a minimum 32 scans and the resolution was ±2 cm^{-1}.

Microstructures of the powders were observed on a JEOL JEM 2100F FETEM instrument. Samples were prepared using a carbon-coated copper grid (150 meshes). Powders were dispersed in ethanol using an ultrasonic horn, and then a drop of the dispersed powder/ethanol mixture was deposited on the grid. The grid was then dried in air. The FETEM was used with an accelerating voltage of 200 kV. The particle size from FETEM micrograph is the average value by statistic method.

Specific surface area analyses were conducted at 77 K using a Norcross ASAP 2010 micromeritics, with N_2 as the absorbate gas. Samples were degassed at 150 °C until the air pressure was below 5 μm Hg. The specific surface areas were calculated using the BET multipoint method with 8 data points. The average particle size of the calcined powders is calculated from specific surface area.

Densities of the sintered specimens were measured by the Archimedes method, using deionized water as the immersion medium. Microstructures of the fractured surfaces and the natural surfaces were observed by EPMA (Model JXA-8100, JEOL, Japan). Mirror-polished samples (1 mm thick) on both surfaces were used to measure the in-line transmittance (Model U-2800 Spectrophotometer, Hitachi, Japan).

3. Results and discussion

Fig. 2 shows the TG/DTA curves of the synthesized precursor. The TG curve showed that complete thermal decomposition of the precursor into oxides was achieved at about 1100 °C with a total mass loss of 35.6% which is higher than the value (19.3%) expected for a precursor of pure hydroxide. Chemical analysis was not performed on the precursor. However, previous work [38,39] revealed that Y^{3+} usually precipitated as basic salt of approximate formula $Y_2(OH)_5NO_3 \cdot nH_2O$ instead of pure hydroxide when ammonia water was used as precipitant. In fact, the mass loss of the present precursor is very close to the theoretical value (34.1%) calculated for $Y_2(OH)_5NO_3 \cdot H_2O$. At the temperature around 111 °C, the endothermic peak with a mass loss of 5.8% appears which is associated to the vaporization of physically bound absorbed water and crystal water. At the temperatures around 310 °C and 543 °C, the two endothermic peaks with a total mass loss of 27.8% were caused by the decomposition of $Y_2(OH)_5NO_3$. The mass loss at the temperature of 1000–1100 °C is mainly due to desulfurization [40].

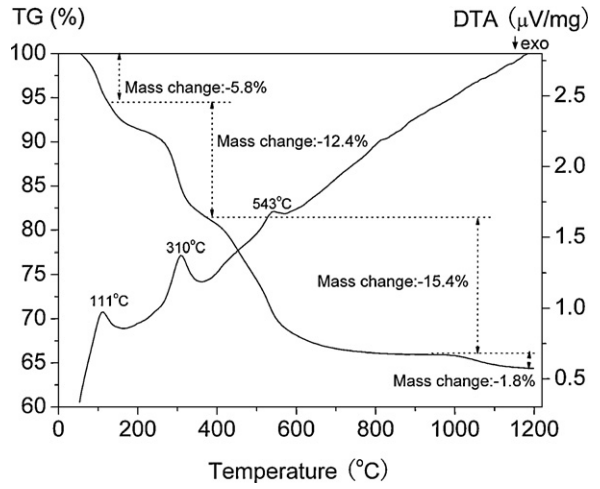

Fig. 2. TG–DTA curves showing the decomposition process of the synthesized precursor.

Table 1
Particle size of the Y_2O_3 powders from precursor calcined at different temperatures.

Y_2O_3	800 °C	900 °C	1000 °C	1100 °C	1200 °C
d_{XRD} (nm)	9	19	35	63	94
d_{TEM} (nm)	27	28	41	67	102
d_{BET} (nm)	45	43	65	101	189

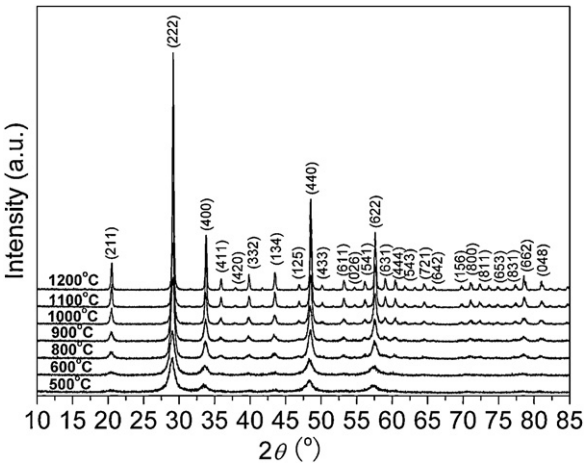

Fig. 3. XRD patterns of the Y_2O_3 powders calcined at different temperatures for 2 h.

XRD patterns of the powders calcined at different temperatures are shown in Fig. 3. At 500 °C, the strongest characteristic peaks of Y_2O_3 phase appear with weak intensity. With increase of the calcination temperature, higher and sharper peaks corresponding to Y_2O_3 with the cubic structure (JCPDS: 895592) observed indicate the improved crystallinity. Crystallite sizes of the Y_2O_3 powders calcined at the temperature range of 800–1200 °C are shown in Table 1. It can be seen that crystallite size increases with increase of calcination temperature. Table 2 shows changes of the cell parameter and the microstrain of Y_2O_3 powders calcined at different temperatures. It is found that the cell constant slightly decreases with increase of temperature up to 900 °C. With further increasing the calcination temperature, the change of the lattice parameter of Y_2O_3 becomes unobvious. A similar trend was recently reported by Saladino et al. [41] on un-doped YAG powders before. For the powders calcined at 1100 and 1200 °C, the cell constants calculated are 10.6108 Å and 10.6014 Å. The values are almost equal to what theoretically it should be (a = 10.604 Å for Y_2O_3, JCPDS No. 25-1200). However, there is an obvious decrease of microstrain with increasing of calcination temperature.

Fig. 4 shows the FTIR spectra of the powders calcined at various temperatures. The absorption band at ~1626 cm^{-1} is characteristic of H–O–H bending mode (ν2) of molecular water. The broad-band peaking at ~3450 cm^{-1} is associated with the coupled effects of molecular water and free hydroxyl groups. Absorption bands at 1550 and 1390 cm^{-1} may be caused by the absorption of H_2O and CO_2 in the synthesized powder. Strong absorption bands in the range of 1000–1280 cm^{-1} were reported for SO_4^{2-} [42]. In addition, the (Y–O) vibration band is clearly observed at ~540 cm^{-1}, suggesting the mass formation of Y_2O_3 along with dehydration and desulfurization. The apparent decomposition temperature of the present sulfate was ~1000 °C, as shown in Fig. 4. Some chemical

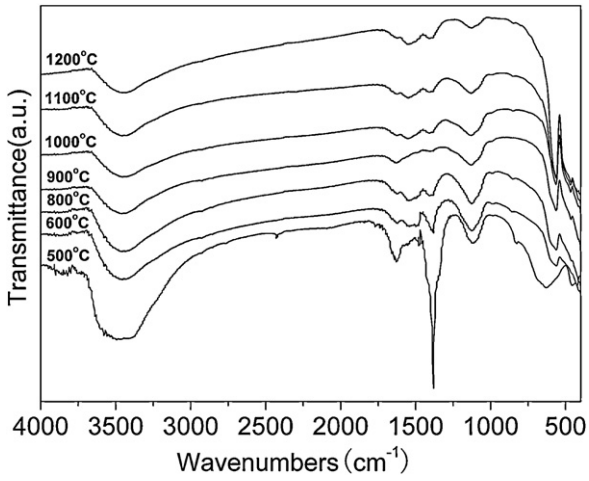

Fig. 4. FTIR patterns of the Y_2O_3 powders calcined at different temperatures for 2 h.

species containing sulfur dissociated from yttria powder, however, even at the temperature of 1200 °C, absorptions corresponding to water, free hydroxyls, CO_2, and SO_4^{2-} are still observed in the powder decomposed at 1200 °C for 2 h, as shown in Fig. 4.

Fig. 5 shows the FETEM micrographs of the synthesized precursor and Y_2O_3 powders calcined at different temperatures for 2 h. The precursor mainly contains sub-micrometer aggregates of nano-sized primary particles. As the calcination temperature was raised, the agglomerated crystallites combined into an individual particle with increasing crystallite size. The particle size from the FETEM observation is shown in Table 1. For comparison, the average particle size derived from the following formula is also shown in Table 1:

$$d_{BET} = \frac{6}{\rho \cdot S_{ssa}}$$

with d_{BET} being the average particle size, ρ the density of the material, and S_{ssa} its specific surface area. It can be concluded that the agglomeration scope for the yttria powder calcined at 1100 °C is relatively lower according to the average crystallite size calculated by XRD and average particle size from FETEM observation or BET calculation. In our experiment, the prepared nano-size yttria particle is not a single crystallite but polycrystallite. The particle calculated by XRD broadening is an average crystallite size of yttria. The particle from FETEM observation is composed of some even smaller crystallites, and particle size is the average value of polycrystallite congeries. So the particle size calculated by XRD is usually smaller than that by FETEM observation, except that every particle is also a crystallite. The particle size calculated using specific surface area value is the equivalent ball diameter of yttria powder, which is usually larger than average crystallite size calculated by XRD broadening.

Using the yttria powder calcined at 1100 °C, commercial α-Al_2O_3, Nd_2O_3 and Cr_2O_3 as the raw materials, 0.1 at.%Cr,1.0 at.%Nd:YAG ceramics were fabricated by solid-state reaction method and vacuum sintering. Fig. 6 shows the XRD patterns of the samples sintered at 1600 °C, 1650 °C, 1700 °C and 1750 °C for 10 h. All the diffraction peaks can be well indexed as the cubic structure of garnet ($Y_3Al_5O_{12}$, JCPDS 82-0575) within XRD

Table 2
Changes of the cell constant and the microstrain of Y_2O_3 powders as a function of calcination temperature.

Y_2O_3	600 °C	800 °C	900 °C	1000 °C	1100 °C	1200 °C
Cell constant (Å)	10.6282	10.6242	10.6160	10.6106	10.6108	10.6014
Microstrain	2.8906E−3	2.3585E−3	1.8497E−3	1.4435E−3	6.6016E−4	3.4426E−4

Table 3
Changes of the cell constant and the microstrain of 0.1 at.%Cr,1.0 at.%Nd:YAG ceramic as a function of calcination temperature.

0.1 at.%Cr,1.0 at.%Nd:YAG	1600 °C	1650 °C	1700 °C	1750 °C
Cell constant (Å)	12.0224	12.0266	12.0274	12.0340
Microstrain	3.6552E−5	7.0546E−5	1.9643E−4	2.6058E−4

detection limit. Changes of the cell constant and the microstrain of 0.1 at.%Cr,1.0 at.%Nd:YAG ceramic as a function of calcination temperature are shown in Table 3. It can be seen that there are slight increase in the lattice constant and obvious decrease in the microstrain with increasing the sintering temperature. YAG ($Y_3Al_5O_{12}$) belongs to the space group I_a3d (O_h^{10}). The standard crystallographic unit cell of YAG is a body-centered cube with a_o = 12.005 Å and contains eight formula units. (There are at least 4

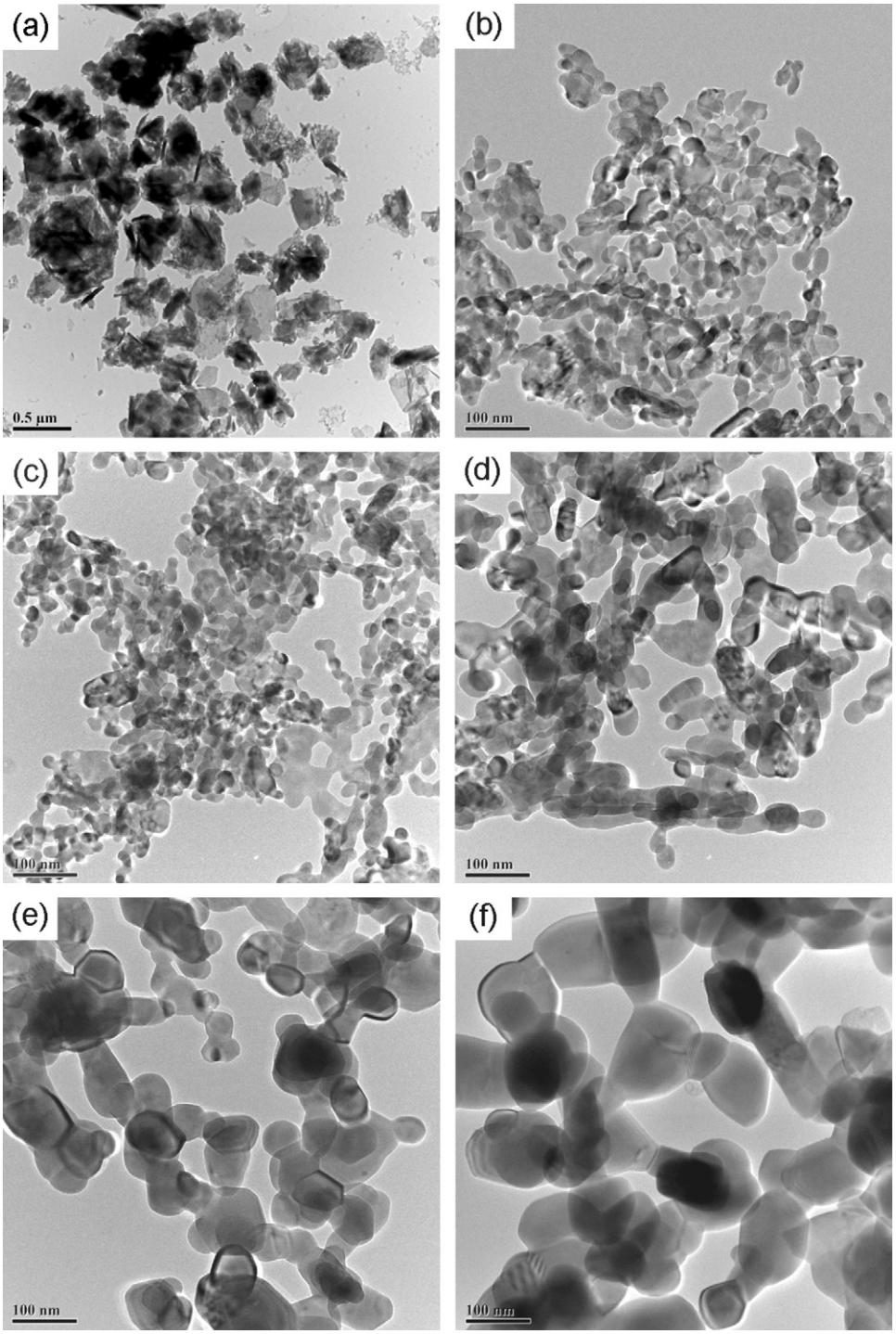

Fig. 5. FETEM micrographs of (a) the synthesized precursor and Y_2O_3 powders from the precursor calcined at (b) 800 °C; (c) 900 °C; (d) 1000 °C, (e) 1100 °C and (f) 1200 °C for 2 h.

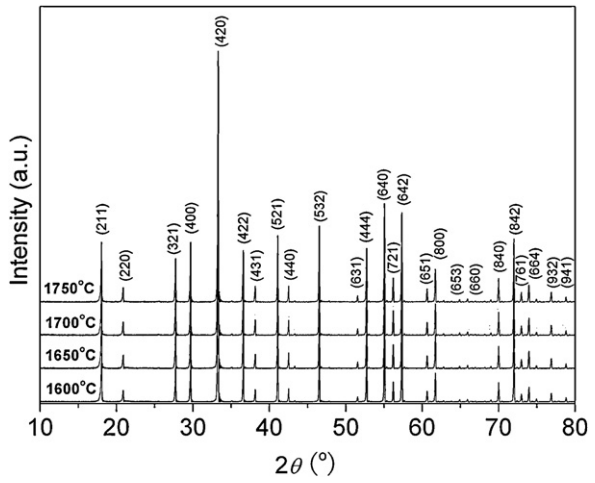

Fig. 6. XRD patterns of the samples sintered at different temperatures for 10 h.

independent lattice parameter evaluations for pure YAG powders in the commercial literature of ICSD: the values are 12.002 Å, 12.004 Å, 12.006 Å and 12.008 Å. In this paper, an average lattice constant of 12.005 Å was used.) The cations are all in special lattice positions labeled as a, b, c with no positional degrees of freedom, while the oxygen atoms locate in the general positions 96(h) [43]. Yttrium occupies dodecahedral 24(c) positions whereas there are two different sites for aluminum ions, namely octahedral 16(a) and tetrahedral 24(d) in the lattice. In YAG lattice, the ionic radius of eightfold coordinated yttrium ions is 0.102 nm and the ionic radii of sixfold and tetrahedrally coordinated aluminum ions are 0.054 nm and 0.039 nm [44]. When divalent calcium ion (Ca^{2+}) is added as a charge compensator, both Cr^{3+} and Cr^{4+} can be introduced in to YAG lattice. The ionic radii of Cr^{3+} and Cr^{4+} are 0.062 nm and 0.041 nm, respectively. So Cr^{3+} and Cr^{4+} are regarded as being substituted into the octahedral Al site and the distorted tetrahedral Al site in the garnet lattice, respectively. The substitution of Cr for Al in $Y_3Cr_yAl_{5-y}O_{12}$ will lead to the slight expansion of YAG lattice. The cell constant of 0.1 at.%Cr:YAG transparent

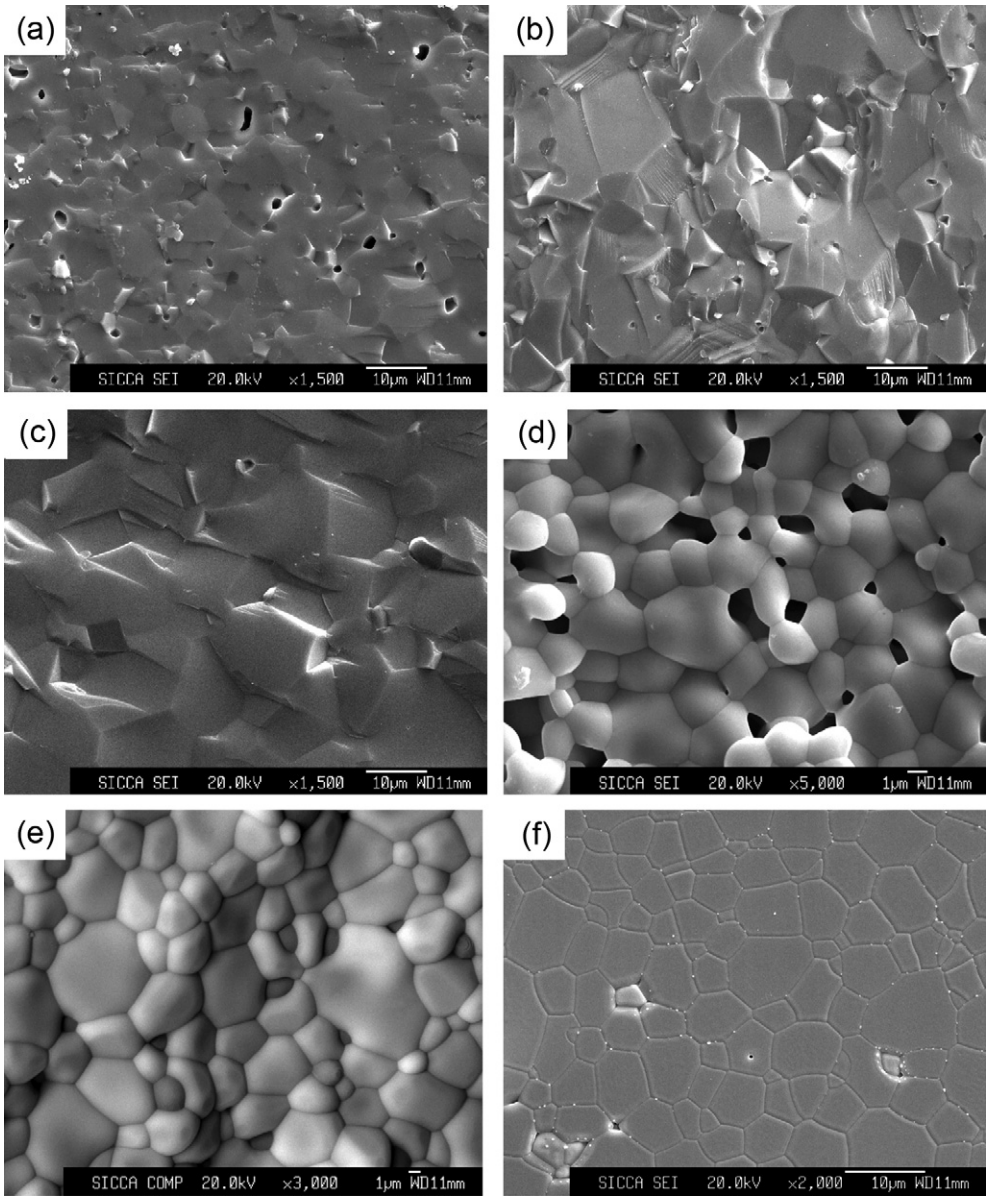

Fig. 7. EPMA micrographs of (a–c) the fractured surfaces of the specimens sintered at 1650 °C, 1700 °C and 1750 °C for 10 h, (d and e) the natural surfaces of the specimens sintered at 1650 °C and 1700 °C for 10 h, and (f) the mirror-polished and thermal etched surface of the sample sintered at 1750 °C for 10 h.

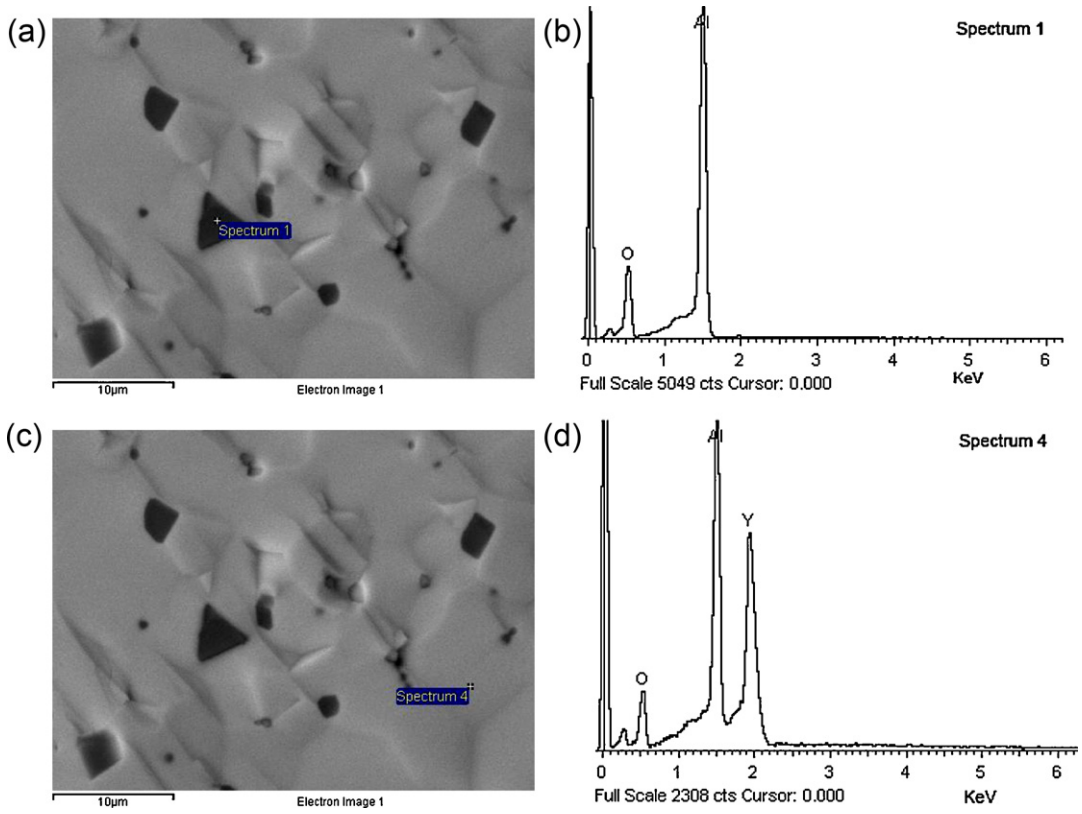

Fig. 8. Back-scattered electron images and energy spectra of the sample sintered at 1700 °C for 10 h using self-synthesized yttria powder as starting material (a and b) secondary phase, (c and d) matrix.

is 12.0094 Å, which is larger than that of YAG. In addition, the ionic radius of Nd^{3+} is 0.112 nm and Nd^{3+} is considered as being substituted into the dodecahedral Y site. It is undoubted that the introduction of Nd^{3+} will also expand the YAG lattice, as can be confirmed by the work reported by Caponetti et al. [45] before. For 1.0 at.%Nd:YAG transparent ceramic, the cell constant is as high as 12.0264 Å. When 0.1 at.%Cr,1.0 at.%Nd:YAG ceramic was sintered at 1600 °C, pure phase of cubic garnet phase formed and partial Nd^{3+}, Cr^{3+} and Cr^{4+} ions entered the YAG lattice. More doping ions went into the YAG lattice and the lattice constant increased from 12.0224 Å to 12.0340 Å with increase of sintering temperature up to 1750 °C. The cell constant of the sample sintered at 1750 °C for 10 h is larger than those of 0.1 at.%Cr:YAG and 1.0 at.%Nd:YAG ceramics. In a large extend, the degree of lattice distortion is influenced by the doping ion quantity in lattice. So the microstrain in Cr,Nd:YAG ceramic distinctly increases with increasing the sintering temperature. Of course, there are many other factors that will influence the micro-strain of YAG lattice. For example, the quantity and the distribution of dislocations, the size and the shape of grains, the quantity, the size, the shape and the distribution of micro-pores, the quantity, the position and the distribution of doping ions and the surface defects and micro-strain of the crushed ceramic powders will all influence the micro-strain of the YAG lattice. Besides, the error of X-ray diffractometer will also influence the peak position and the peak width.

Fig. 7 shows the EPMA micrographs of the samples sintered at different temperatures for 10 h. It can be seen from the micrographs of the fracture surfaces that grain size increases with increase of sintering temperature. Obvious pore removal occurs between 1650 and 1700 °C, which can be detected from the EPMA micrographs of the natural surfaces. A dense and nearly pore-free surface-microstructure of sample was observed at 1700 °C. However, even at 1750 °C, there are still some residual pores at the grain boundaries or inner grains observed from the mirror-polished and thermal etched surface of the sample. It can be seen that the specimen displays average grain size of about 8 μm. With further increase the sintering temperature to 1780 °C, the sample would be over-sintered and no grains could be found from the EPMA microscope observations. By using commercial yttria powder as starting material, very dense and nearly pore-free microstructures of 0.1 at.%Cr,1.0 at.%Nd:YAG ceramics solid-state-reactive-sintered at 1750 °C, 1780 °C and 1800 °C for 10 h could be obtained [30,31]. It is found that the use of nano-sized yttria powder instead of commercial large-scaled yttria powder can effectively decrease the sintering temperature to a certain degree because of the high reaction and sintering activity of nano-yttria powder. Nevertheless, more micro-pores were remained at the grain boundaries or inner grains in the present fabrication process. This may be caused by the low green density and over-quick solid-state-reaction and grain growth speed. Only by optimizing the fabrication process, such as increasing the green density and controlling the grain growth and grain boundary migration speed, pore-free structure Cr^{4+},Nd^{3+}:YAG ceramics could be obtained. However, for the sample sintered at 1750 °C using self-synthesized yttria powder as starting material, it is still confusing that the optical transmittance of the sample is relatively low, although there are not so many micro-pores at the grain boundaries or inner grains. So back-scattered electron image and energy spectrum observations of the sample sintered at 1700 °C was done to validate whether there was secondary phase or not. It can be considered from Fig. 8 that the formation of secondary phase corresponding to alumina is caused by the decomposition of SO_4^{2-} ions in yttria powder and the absorption of water by yttria nanopowder, which has led to nonstoichiometry of 0.1 at.%Cr,Nd:YAG, when the prepared nano-sized yttria powder reacted with other oxide powders. For the sample sintered at 1750 °C, there were few micro-pores, however,

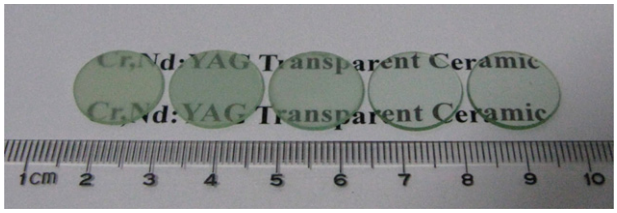

Fig. 9. Photo of the of the mirror-polished 0.1 at.%Cr,1.0 at.%Nd:YAG transparent ceramics sintered at (a) 1650 °C, (b) 1700 °C, (c) 1750 °C (using wet-chemical synthesis nano-yttria powder), (d) 1750 °C and (e) 1780 °C for 10 h (using commercial large-scaled yttria powder).

the secondary phase of alumina was still remained. However, the content of the secondary phase is too small to be detected by XRD observation, because it is out of the XRD detection limit.

Fig. 9 shows the photo of the of the mirror-polished 0.1 at.%Cr,1.0 at.%Nd:YAG transparent ceramics sintered at 1650 °C, 1700 °C, and 1750 °C for 10 h (using wet-chemical synthesis nano-yttria powder), and 1750 °C and 1780 °C for 10 h using commercial large-scaled yttria powder as starting material. The thickness of all the samples is 1.0 mm. Fig. 10 shows the optical transmittances of the samples sintered at 1650 °C, 1700 °C and 1750 °C for 10 h using nano-yttria powder as raw material. The in-line transmittance increases with increase of sintering temperature. For the sample sintered at 1750 °C for 10 h, the transmittance reached 52% at 1064 nm. However, the value of transmission is much lower than the theoretical value. With further increase the sintering temperature to 1780 °C, the over-sintered sample became completely opaque. The low transparency of Cr^{4+},Nd^{3+}:YAG ceramics is due to the existence of secondary phase and the remained micro-pores. Only through properly adjusting the nano-sized yttria addition and controlling the preparing process, the secondary phase can be eliminated, the micro-pores can be further decreased and the optical transmittance of the sample can be greatly improved. For comparison, in-line transmittances of the Cr^{4+},Nd^{3+}:YAG ceramics vacuum-sintered at 1750 °C and 1780 °C using commercial large-scaled yttria powder as raw material is shown in Fig. 11. It is found that the transmittances of the samples are 80.8% and 82.1% at 1064 nm, respectively, which are much higher than those of samples with nano-yttria as starting powder. In order to improve the transparency of the samples fabricated using nano-sized and homogeneous yttria powder as one of the starting materials, weight loss cause by the decomposition of SO_4^{2-} ions and the absorption of water or organic materials in yttria nanopowder should be taken into account.

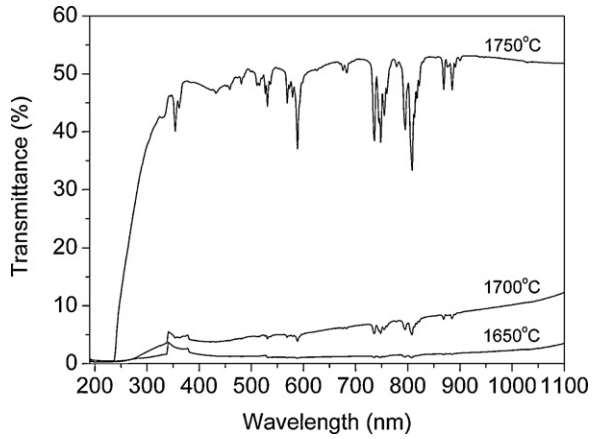

Fig. 10. Optical transmittances of the mirror-polished 0.1 at.%Cr,1.0 at.%Nd:YAG transparent ceramics sintered at (a) 1650 °C, (b)1700 °C and (c)1750 °C for 10 h (using wet-chemical synthesis nano-yttria powder).

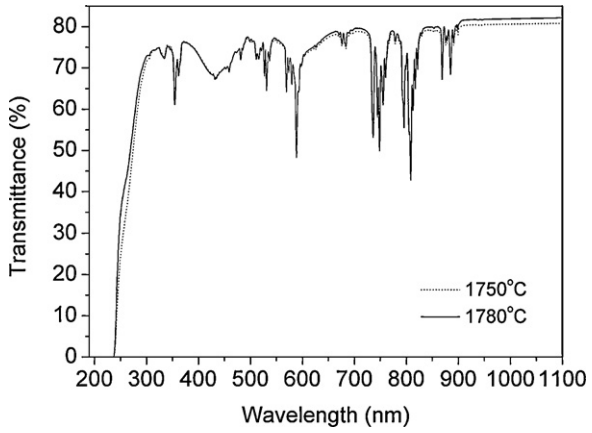

Fig. 11. Optical transmittances of the mirror-polished 0.1 at.%Cr,1.0 at.%Nd:YAG transparent ceramics sintered at (a) 1750 °C (dashed line) and (b)1780 °C (solid line) for 10 h (using commercial large-scaled yttria powder).

4. Conclusions

Nanocrystalline yttria powders were synthesized by a precipitation method from yttrium nitrate solution with ammonia water as a precipitant. Using the prepared nanometer Y_2O_3, and the high-purity commercial powders of α-Al_2O_3, Nd_2O_3 and Cr_2O_3 as raw materials, Cr,Nd:YAG transparent ceramic was fabricated by a solid-state reaction and vacuum sintering. The results of the present study can be summarized as follows:

(1) It was found that the addition of small amount of ammonia sulfate in yttrium nitrate solution can reduce the agglomeration of the produced yttria powders.
(2) Fine and low-agglomeration yttria powder with an average particle size of 67 nm was obtained by calcining the precursor at 1100 °C for 2 h.
(3) The transparent Cr,Nd:YAG ceramic obtained by sintering at 1750 °C for 10 h exhibited a dense and homogeneous microstructure with secondary phase of alumina. The secondary phase was caused by the desulfurization and absorbed water evaporation of the prepared nano-yttria powder.
(4) The in-line transmittance of the Cr,Nd:YAG ceramic sintered at 1750 °C for 10 h reached 52% at 1064 nm, which was much lower than that of the sample (82.1%) sintered at 1780 °C for 10 h using all-commercial powders as starting materials. The low transmittance was mainly due to the existence of secondary phase.
(5) Through further optimizing the fabrication process, Cr,Nd:YAG transparent ceramics with high optical quality could be obtained, which is a potential self-Q-switched laser material used for generating sub-nanosecond laser pulses.

Acknowledgements

This work was supported by the Natural Science Foundation of Shanghai (Grant No. 10ZR1433900), the Project for Young Scientists Fund of National Natural Science Foundation of China (Grant No. 51002172), the Key Program of National Natural Science Foundation of China (Grant No. 91022035) and the Science and Technology Innovation Program of Shanghai Institute of Ceramics, Chinese Academy of Sciences (Grant No. Y12ZC3130G). We are grateful to Dr. Haohong Chen for the assistance in XRD study and helpful discussion.

References

[1] A. Ikesue, T. Kinoshita, K. Kamata, K. Yoshida, J. Am. Ceram. Soc. 78 (1995) 1033–1040.
[2] I. Shoji, S. Kurimura, Y. Sato, T. Taira, Appl. Phys. Lett. 77 (2000) 939–941.
[3] J. Lu, M. Prahu, J. Xu, K. Ueda, H. Yagi, T. Yanagitani, A.A. Kaminskii, Appl. Phys. Lett. 77 (2000) 3707–3709.
[4] S.H. Lee, S. Kochawattana, G.L. Messing, J. Am. Ceram. Soc. 89 (2006) 1945–1950.
[5] H. Yagi, K. Takaichi, K. Hiwada, K. Ueda, T. Yanagitani, Jpn. J. Appl. Phys. 45 (2006) L207–L209.
[6] A. Ikesue, Y.L. Aung, J. Am. Ceram. Soc. 89 (2006) 1936–1944.
[7] J. Li, Y.S. Wu, Y.B. Pan, W.B. Liu, L.P. Huang, J.K. Guo, Int. J. Appl. Ceram. Technol. 5 (2008) 360–364.
[8] A. Ikesue, Y.L. Aung, Nat. Photon. 2 (2008) 721–728.
[9] S.H. Zhou, K.K. Lee, Y.C. Chen, Opt. Lett. 18 (1993) 511–512.
[10] Y.C. Chen, S. Li, K.K. Lee, S. Zhou, Opt. Lett. 18 (1993) 1418–1419.
[11] J. Dong, P.Z. Deng, Y.T. Lu, Y.H. Zhang, Y.P. Liu, J. Xu, W. Chen, Opt. Lett. 25 (2000) 1101–1103.
[12] Y.S. Wu, J. Li, Y.B. Pan, Q. Liu, J.K. Guo, B.X. Jiang, J. Xu, J. Am. Ceram. Soc. 90 (2007) 1629–1631.
[13] T.D. Huang, B.X. Jiang, Y.S. Wu, J. Li, Y. Shi, W.B. Liu, Y.B. Pan, J.K. Guo, J. Alloys Compd. 478 (2009) L16–L20.
[14] X.D. Li, J.G. Li, Z.M. Xiu, D. Huo, X.D. Sun, J. Am. Ceram. Soc. 92 (2009) 241–244.
[15] W.X. Zhang, J. Zhou, W.B. Liu, J. Li, L. Wang, B.X. Jiang, Y.B. Pan, X.J. Cheng, J.Q. Xu, J. Alloys Compd. 506 (2010) 745–748.
[16] Y.K. Li, S.M. Zhou, H. Lin, X.R. Hou, W.J. Li, H. Teng, T.T. Jia, J. Alloys Compd. 502 (2010) 225–230.
[17] E.R. Kupp, G.L. Messing, J.M. Anderson, V. Gopalan, J.Q. Dumm, C. Kraisinger, N. Ter-Gabrielyan, L.D. Merkle, M. Dubinskii, V.K. Simonaitis-Castillo, G.J. Quarles, J. Mater. Res. 25 (2010) 476–483.
[18] H. Yang, X.P. Qin, J. Zhang, S.W. Wang, J. Ma, L.X. Wang, Q.T. Zhang, J. Alloys Compd. 509 (2011) 5274–5279.
[19] F. Tang, Y.G. Cao, W. Guo, Y.J. Chen, J.Q. Huang, Z.H. Deng, Z.G. Liu, Z. Huang, Opt. Mater. 33 (2011) 1278–1282.
[20] H. Yang, X.P. Qin, J. Zhang, J. Ma, D.Y. Tang, S.W. Wang, Q. Zhang, Q.T. Zhang, Opt. Mater. (2011), doi:10.1016/j.optmat.2011.05.029.
[21] W.B. Liu, J. Li, B.X. Jiang, D. Zhang, Y.B. Pan, J. Alloys Compd. 25 (2011) 1–4.
[22] J. Li, J. Zhou, Y.B. Pan, W.B. Liu, W.X. Zhang, J.K. Guo, H. Chen, D.Y. Shen, X.F. Yang, T. Zhao, J. Am. Ceram. Soc. (2011), doi:10.1111/j.1551-2916.2011.04915.x.
[23] J.G. Li, T. Ikegami, J.H. Lee, T. Mori, J. Am. Ceram. Soc. 83 (2000) 961–963.
[24] X. Li, Q. Li, J.Y. Wang, S.L. Yang, H. Liu, Opt. Mater. 29 (2007) 528–531.
[25] W.B. Liu, W.X. Zhang, J. Li, H.M. Kou, Y.Q. Shen, L. Wang, Y. Shi, D. Zhang, Y.B. Pan, J. Alloys Compd. 503 (2010) 525–528.
[26] W.B. Liu, W.X. Zhang, J. Li, H.M. Kou, D. Zhang, Y.B. Pan, J. Eur. Ceram. Soc. 31 (2011) 653–657.
[27] Y.H. Sang, H. Liu, X.D. Sun, X.L. Zhang, H.M. Qin, Y.H. Lv, D. Huo, D. Liu, J.Y. Wang, R.I. Boughton, J. Alloys Compd. 509 (2011) 2407–2413.
[28] X.L. Zhang, D. Liu, Y.H. Sang, H. Liu, J.Y. Wang, J. Alloys Compd. 502 (2010) 206–210.
[29] M. Suárez, A. Fernández, J.L. Menéndez, R. Torrecillas, J. Alloys Compd. 493 (2010) 391–395.
[30] J. Li, Y.S. Wu, Y.B. Pan, J.K. Guo, J. Non-Cryst. Solids 352 (2006) 2404–2407.
[31] J. Li, Y.S. Wu, Y.B. Pan, H.M. Kou, Y. Shi, J.K. Guo, Ceram. Int. 34 (2008) 1675–1679.
[32] J. Li, Y.S. Wu, Y.B. Pan, W.B. Liu, Y. Zhu, J.K. Guo, J. Ceram. Soc. Jpn. 116 (2008) 572–577.
[33] L. Wen, X.D. Sun, Z.M. Xiu, X.W. Chen, C.T. Tsai, J. Eur. Ceram. Soc. 24 (2004) 2681–2688.
[34] J. Li, Y.S. Wu, Y.B. Pan, L.Q. An, J. Zhang, S.W. Wang, J.K. Guo, J. Inorg. Mater. 22 (2007) 798–802.
[35] J. Li, Y.S. Wu, Y.B. Pan, W.B. Liu, L.Q. An, S.W. Wang, J.K. Guo, J. Chin. Ceram. Soc. 35 (2007) 1600–1604.
[36] Y.S. Wu, J. Li, Y.B. Pan, J.K. Guo, B.X. Jiang, Y. Xu, H.B. Yu, X.Y. Liang, J. Xu, J. Am. Ceram. Soc. 90 (2007) 3334–3337.
[37] J. Li, Y.S. Wu, Y.B. Pan, W.B. Liu, L.P. Huang, J.K. Guo, Opt. Mater. 31 (2008) 6–17.
[38] C.E. Holcombe, J. Am. Ceram. Soc. 61 (1978) 481–486.
[39] J.G. Li, T. Ikegami, J.H. Lee, T. Mori, Y. Yajima, J. Eur. Ceram. Soc. 20 (2000) 2395–2405.
[40] T. Ikegami, J.G. Li, T. Mori, Y. Moriyoshi, J. Am. Ceram. Soc. 85 (2002) 1725–1729.
[41] M.L. Saladino, E. Caponetti, D.C. Martino, S. Enzo, G. Ibba, Opt. Mater. 31 (2008) 261–267.
[42] J.G. Li, T. Ikegami, T. Mori, J. Am. Ceram. Soc. 88 (2005) 817–821.
[43] M.M. Kuklja, J. Phys.: Condens. Mater. 12 (2000) 2953–2967.
[44] X.Q. Feng, Laser Optoelectron. Prog. 43 (2006) 19–28.
[45] E. Caponetti, M.L. Saladino, F. Serra, S. Enzo, J. Mater. Sci. 42 (2007) 4418–4427.